Received: 6 February 2019 | Revised: 10 July 2019 | Accepted: 12 July 2019

DOI: 10.1111/bph.14808

RESEARCH PAPER

Inhibition of the hyaluronan matrix enhances metabolic anticancer therapy by dichloroacetate in vitro and in vivo

Sören Twarock | Christina Reichert | Katharina Bach | Oliver Reiners | Inga Kretschmer | Daniel J. Gorski | Katharina Gorges | Maria Grandoch | Jens W. Fischer

Institut für Pharmakologie und Klinische Pharmakologie, Universitätsklinikum der Heinrich-Heine-Universität, Düsseldorf, Germany

Correspondence
Sören Twarock, Institut für Pharmakologie und Klinische Pharmakologie, Universitätsklinikum der Heinrich-Heine-Universität, Düsseldorf, Germany.
Email: soeren.twarock@uni-duesseldorf.de

Funding information
Forschungskommission der Heinrich-Heine-Universität Düsseldorf, Grant/Award Number: 51/2015

Background and Purpose: Aerobic glycolysis is a unique feature of tumour cells that entails several advantages for cancer progression such as resistance to apoptosis. The low MW compound, dichloroacetate, is a pyruvate dehydrogenase kinase inhibitor, which restores oxidative phosphorylation and induces apoptosis in a variety of cancer entities. However, its therapeutic effectiveness is limited by resistance mechanisms. This study aimed to examine the role of the anti-apoptotic hyaluronan (HA) matrix in this context and to identify a potential add-on treatment option to overcome this limitation.

Experimental Approach: The metabolic connection between dichloroacetate treatment and HA matrix augmentation was analysed in vitro by quantitative PCR and affinity cytochemistry. Metabolic pathways were analysed using Seahorse, HPLC, fluorophore-assisted carbohydrate electrophoresis, colourimetry, immunoblots, and immunochemistry. The effects of combining dichloroacetate with the HA synthesis inhibitor 4-methylumbelliferone was evaluated in 2D and 3D cell cultures and in a nude mouse tumour xenograft regression model by immunoblot, immunochemistry, and FACS analysis.

Key Results: Mitochondrial reactivation induced by dichloroacetate metabolically activated HA synthesis by augmenting precursors as well as O-GlcNAcylation. This process was blocked by 4-methylumbelliferone, resulting in enhanced anti-tumour efficacy in 2D and 3D cell culture and in a nude mouse tumour xenograft regression model.

Conclusions and Implications: The HA rich tumour micro-environment represents a metabolic factor contributing to chemotherapy resistance. HA synthesis inhibition exhibited pronounced synergistic actions with dichloroacetate treatment on oesophageal tumour cell proliferation and survival in vitro and in vivo suggesting the combination of these two strategies is an effective anticancer therapy.

Abbreviations: 4-MU, 4-methylumbelliferone; CK18, cytokeratin 18; ECM, extracellular matrix; ESCC, oesophageal squamous cell carcinoma; FACE, fluorophore-assisted carbohydrate electrophoresis; G6P, glucose 6-phosphate; GlcNAc, *N*-acetyl-glucosamine; HA, hyaluronan; HAbP, HA binding protein; HAS, hyaluronan synthase; HYAL, hyaluronidase; OXPHOS, oxidative phosphorylation; PDC, pyruvate dehydrogenase complex; PDK, pyruvate dehydrogenase kinase; RHAMM, receptor for hyaluronan-mediated motility

Sören Twarock and Christina Reichert should be considered joint first authors.

1 | INTRODUCTION

Cancer cell metabolism has regained substantial attention as a potential drug target that distinguishes cancer cells from their non-malignant counterparts. Several new strategies have emerged and have provided promising new anticancer drugs (Martinez-Outschoorn, Peiris-Pages, Pestell, Sotgia, & Lisanti, 2017; Vernieri et al., 2016). One of the most evident characteristics of cancer cells is the metabolic switch from oxidative phosphorylation (OXPHOS) to aerobic glycolysis, which was first described by the Nobel laureate Otto Warburg, hence termed the Warburg effect (Warburg, 1956). It originates in reduced activity of the **pyruvate dehydrogenase complex** (PDC), which facilitates the conversion of pyruvate to acetyl-CoA and thus sustains mitochondrial OXPHOS. In a range of cancer cells, the activity of PDC is impeded by an increased **pyruvate dehydrogenase kinase** (PDK) activity, resulting in reduced mitochondrial activity. To compensate for the loss in ATP synthesis by mitochondrial OXPHOS, the glycolytic flux is increased, finally resulting in a much increased generation of lactate. Even though energy homeostasis is impaired by this process, the advantages for the growing cancer cell seem to outweigh this limitation. Inhibition of mitochondria-originated apoptosis, accumulation of biomass from early glucose metabolites, and creation of an acidified extracellular micro-environment are presumably supportive for tumour growth and spread (Vander Heiden, Cantley, & Thompson, 2009).

Intensive research on the Warburg effect led to the discovery of the low MW compound dichloroacetate, which was first used to reduce plasma glucose and triglycerides in patients with diabetes and hyperlipoproteinaemia (Stacpoole, Moore, & Kornhauser, 1978). In more recent years, it has been tested as an orphan drug to treat genetic mitochondrial diseases (Stacpoole, Kurtz, Han, & Langaee, 2008) such as lactate acidosis in children (Stacpoole et al., 2006) and the MELAS syndrome (Kaufmann et al., 2006). It was not before 2007 that dichloroacetate was also shown to reverse anaerobic glycolysis in tumour cells by dephosphorylation of PDK. This effect restores PDC activity, which enables reactivation of mitochondria and eventually results in the induction of mitochondria-driven apoptosis in transformed cells (Bonnet et al., 2007; Michelakis, Webster, & Mackey, 2008). As cell culture (Table S3) and animal experiments (Table S4) showed a considerable activity of this compound against a variety of tumour entities, dichloroacetate has gained wide attention in the scientific community in recent years (Kankotia & Stacpoole, 2014). Even though clinical studies confirm an overall good safety profile of dichloroacetate in humans, peripheral neuropathy emerged as the prominent dose-limiting side effect that often required dose reduction resulting in a loss of efficacy (Kaufmann et al., 2006). For instance, in recent phase I studies in NSCLC and glioblastoma patients, an effective dosage of 25–50 $mg \cdot kg^{-1} \cdot day^{-1}$ was defined, but severe reversible neuropathy was reported in 38–86% of patients (Dunbar et al., 2014; Garon et al., 2014; Michelakis et al., 2010). A reduction of the dichloroacetate dose to 6.5–12.5 $mg \cdot kg^{-1} \cdot day^{-1}$ generally ameliorated the emergence of this side effect but led to a loss of tumour growth reduction (Chu et al., 2015; Garon et al., 2014; Michelakis et al., 2010). Given these clinical results, there is a keen interest in exploring the mechanisms behind the diminished response to dichloroacetate treatment and in finding synergistic combination partners for therapy with dichloroacetate (Chu et al., 2015; Kaufmann et al., 2006; Sun, Board, & Blackburn, 2011; Zhou et al., 2015).

What is already known

- Dichloroacetate is a promising metabolic chemotherapeutic agent, but its efficacy needs further improvement.
- The hyaluronan matrix provides antiapoptotic signals via hyaluronan receptors.

What this study adds

- Dichloroacetate treatment triggers hyaluronan synthesis metabolically via Krebs cycle activation.
- 4-Methylumbelliferone inhibits hyaluronan synthesis and counteracts this process, thus synergistically enhancing the efficacy of dichloroacetate.

What is the clinical significance

- Both dichloroacetate and 4-methylumbelliferone, have been used in humans and show a favourable safety profile.
- This drug combination may represent a promising therapeutic option for tumours exhibiting the Warburg effect.

In order to identify potential compounds that enhance the efficacy of dichloroacetate or other strategies aiming at the restoration of mitochondrial OXPHOS, we focused on the extracellular matrix (ECM) as it is a pivotal component of the tumour stroma by forming a supportive tumour micro-environment (Pickup, Mouw, & Weaver, 2014). Specifically, we investigated the role of the ECM component hyaluronan (HA) as its synthesis is closely coupled to glycolysis intermediates (Moretto et al., 2015; Tammi et al., 2011; Twarock et al., 2017) and its abundance in the vicinity of cancer cells is a hallmark of tumour development, which has been shown to support tumour growth and spread, metastasis, chemotherapy resistance, and anti-apoptosis (Chanmee, Ontong, & Itano, 2016; Tammi et al., 2018). These processes are mediated by HA receptors, for example, CD44 and the receptor for hyaluronan-mediated motility (RHAMM), which trigger potent anti-apoptotic signalling pathways (Misra, Hascall, Markwald, & Ghatak, 2015). HA is an unbranched polysaccharide that is composed of alternating disaccharide units of **glucuronic acid** and *N*-acetyl-glucosamine (GlcNAc) and is synthesized by three membrane-bound isoforms of the HA synthase family (HAS1-3; Itano et al., 1999). Its synthesis can be inhibited by the orally available compound 4-methylumbelliferone (4-MU), which depletes the activated uridine diphosphate (UDP)-glucuronic acid precursor pool and thus interferes with HA production (Kakizaki et al., 2004). The efficacy of 4-MU in reducing the growth of a variety of tumour cells lines is well

documented (Table S5). In animal experiments, 4-MU was shown to attenuate tumour progression of, for example, oesophageal squamous cell carcinoma (ESCC) cells (Twarock et al., 2011; Twarock et al., 2017), hepatoma cells (Piccioni et al., 2015), bladder cancer cells (Morera et al., 2017), and prostate cancer cells (Lokeshwar et al., 2010). Moreover, it reduced metastatic spread of melanoma cells (Yoshihara et al., 2005) and chemotherapy resistance of pancreatic cancer cells (Nakazawa et al., 2006) and breast cancer cells (Chen & Bourguignon, 2014; Palyi-Krekk et al., 2007). For further references, see also Table S6. Current research is aiming at identifying diseases and conditions in which 4-MU may present a valuable treatment option (Twarock et al., 2017).

For discovering a potential resistance mechanism involving the tumour micro-environment, we first investigated the effects of a dichloroacetate-induced restoration of the mitochondrial activity on the anti-apoptotic HA system. Subsequently, we established a mechanism that describes how reactivation of OXPHOS triggers HA synthesis (HAS) in two different ways. As proof of concept, we show that the inhibition of this process is effective to synergistically enhance dichloroacetate actions in terms of enhanced apoptosis in 2D and 3D cell cultures in vitro and in a nude mouse tumour xenograft regression model in vivo.

Our results provide insight in the counter-regulatory processes that emerge from the restoration of mitochondrial OXPHOS and show that the combination of dichloroacetate and 4-MU may be a promising pharmacological strategy for treatment of cancer entities exhibiting the Warburg effect. Our data suggest the combination of these two orally available compounds with a good safety profile in humans should be further investigated in clinical trials.

2 | METHODS

2.1 | Cell culture

The human ESCC cell line KYSE-410 (DSMZ Cat# ACC-381, RRID: CVCL_1352; Braunschweig, Germany) was used to perform all experiments and was authenticated by short tandem repeat analysis. Cells were passaged in RPMI-1640 GlutaMAX medium (LifeTechnologies, Carlsbad, USA) containing 10% FBS supplemented with penicillin and streptomycin at 37°C in 5% CO_2 and 95% humidity. The number of viable cells was determined using a Countess cell counter (ThermoFisher, Waltham, USA). Cells were incubated with dichloroacetate in a concentration of 10, 20, or 40 mM as well as either 0.3- or 0.5-mM 4-MU, alone or in combination. With regard to dichloroacetate, we confirmed the doses to be used, with respect to growth inhibition (Figure S1) and the induction of a metabolic shift in our model cell line by quantification of lactate (Figure 2a) and mitochondrial ATP production (Figure 2b). For the experiments on the metabolic mechanism underlying elevated HAS under dichloroacetate, we chose the higher 40-mM dose as it produced a more striking metabolic phenotype (elevation of **glucose 6-phosphate** (G6P), acetyl-CoA, UDP-GlcNAc, and pericellular HA staining) than did the 20-mM dose. Of note, even this strong induction of acetyl-CoA and HA in the medium was rescued by application of the ATP citrate lyase inhibitor SB-204990. For the experiments on in vitro tumour growth inhibition, we decided to use the mid-range concentration of 20-mM dichloroacetate, as this dose showed synergism with 300-μM 4-MU (Table S2) and we sought to explore in this study whether addition of 4-MU can reduce the dichloroacetate dose needed to achieve tumour growth inhibition. 4-MU alone only inhibited cell growth in a concentration of 300 μM (Figure 4a). As higher doses can also impair the synthesis of other glycosaminoglycans (unpublished data), we chose this dose as the highest concentration in our study. Based on the synergism calculation on growth reduction (Table S2) and our previous publications (Twarock et al., 2011; Twarock et al., 2017), we chose the 300-μM dose for further experiments.

2.2 | Animals

All animal care and experimental procedures were approved by the competent animal welfare authority (LANUV NRW) and the institutional animal welfare officer of the University of Düsseldorf under the administrative number 84.02.04.2013.A472 and performed according to the German and European animal welfare law. Animal studies are reported in compliance with the ARRIVE guidelines (Kilkenny et al., 2010; McGrath & Lilley, 2015) and with the recommendations made by the *British Journal of Pharmacology*. Male Crl: NMRI-*Foxn1*^{nu} mice were obtained from Charles River (IMSR Cat# CRL:639, RRID:IMSR_CRL:639; Wilmington, USA) and used for the experiments at the age of 4–6 weeks and a weight of 31.5 g ± 2 g. This mouse strain is commonly used for tumour xenograft experiments. The animals were bred and housed at the central animal housing facility of the Heinrich-Heine-University of Düsseldorf under specific pathogen-free conditions with standard housing and bedding material with four animals per cage. The mice had free access to nude mouse chow with chocolate aroma (Sniff, Soest, Germany) and water. In the groups receiving 4-MU, the drug was pelleted into the chow (see below); in the groups receiving dichloroacetate, the drug was dissolved in the drinking water. The animals were randomized to either treatment group. At the end of the experiment or if abort criteria were met (unusual behaviour as signs of pain or discomfort, tumour size exceeding 15 mm in any direction), the mice were killed by CO_2. Power analyses with $\alpha = .05$ and $1-\beta = .90$ using an estimated effect size of 1 (based on previous studies) yielded a minimum necessary sample size of 8 animals per treatment group.

2.3 | Tumour xenograft regression model

Tumour xenografts were induced by subcutaneous injection of 10^6 KYSE-410 cells into both flanks of the mice. After the injection, the tumour growth was assessed every second day, and the mice were randomized to the treatment groups placebo (nude mice standard chow with chocolate flavour), dichloroacetate, 4-MU, and dichloroacetate + 4-MU when the tumour volume reached at least

30 mm^3. The tumour volume was calculated by caliper measurements with the formula Height × Length × Depth × 0.5. Dichloroacetate was added to the drinking water at a concentration of 0.3 $g \cdot L^{-1}$. Measurement of the volume of water consumed showed that the amount of dichloroacetate administered to each mouse was approximately equal to 50 $mg \cdot kg^{-1}$ body $weight \cdot day^{-1}$. Here, we used a dichloroacetate dose that is established in the literature showing considerable effects on tumour growth in nude mouse xenograft models (Table S4). As in the in vitro experiments, we have chosen a dose of the lower range of published doses (Ishiguro, Ishiguro, Ishiguro, & Iwai, 2012; Ohashi et al., 2013). This dose was also used in clinical studies (Michelakis et al., 2010). 4-MU (AlfaAesar, ThermoFisher) was pelleted into the chow at a concentration of 50 $g \cdot kg^{-1}$ (ssniff, Soest, Germany), which corresponds to a dose of 10 $g \cdot kg^{-1}$ body $weight \cdot day^{-1}$. The 4-MU dose used here was first established by our group in a cardiovascular mouse model, in which the resulting plasma levels of 4MU (600 nM in blood plasma of mice) and the inhibition of HA synthesis were verified (Nagy et al., 2010). In two subsequent studies, our group confirmed the efficacy of this dose to inhibit tumour growth (Twarock et al., 2011; Twarock et al., 2017).

After the start of the treatment, the tumour growth was assessed every fifth day up to 60 days. At the end of the experiment, the mice were killed, and the tumours were excised and embedded for immunostaining. The mice had open access to food and pathogen-free water and were kept at a 12-hr day/night rhythm. All animal experiments were approved by the local animal facility and the responsible animal protection authority.

2.4 | HA assay

Cells were plated in 12-well dishes on glass cover slides and grown to 50% confluence. Next, the cells were incubated with dichloroacetate for 72 hr and fixed. HA was visualized using 1:200 biotinylated HA-binding protein (385911; Calbiochem, San Diego, USA) and 1:1,000 Streptavidin-Cy3 (SA1010; Invitrogen, Carlsbad, USA) in PBS. Nuclei were stained with Hoechst 33342 (H3570; Invitrogen). The HA deposition was calculated as integrated density and normalized to nuclei count using Fiji (Fiji, RRID:SCR_002285; Schindelin et al., 2012). HA content of the supernatant was measured after 72 hr by an ELISA-like immunoaffinity assay (Corgenix, Broomfield, USA). Concentrations were normalized to protein content measured by Bradford assay.

2.5 | Quantitative real-time PCR

Total RNA was isolated after 72 hr of dichloroacetate treatment, and cDNA was synthesized from 1-μg RNA as described previously (Twarock, Tammi, Savani, & Fischer, 2010). The PCR reactions were performed according to standard procedures with SYBR Green PCR Master Mix (Applied Biosystems, Waltham, MA, USA). Relative expression levels were compared by using real-time PCR with the $2^{-\text{??}Ct}$ method. Primer sequences are given in Table S1.

2.6 | Quantification of metabolites

Intracellular acetyl-CoA and G6P were quantified using a colorimetric assay (Sigma) and normalized to total protein content. The ATP citrate lyase inhibitor SB-204990 (TOCRIS, Bristol, UK) was used as a negative control for the acetyl-CoA quantification. Fluorophore-assisted carbohydrate electrophoresis (FACE) was used to quantify intracellular (UDP)-sugars and executed as described previously (Twarock et al., 2017). Signal intensities were quantified by the Software Vision Works (Analytik Jena, Jena, Germany) and normalized to DNA content determined by Quant-iT PicoGreen dsDNA Assay Kit (Invitrogen).

2.7 | Real-time metabolism analysis

Oxygen consumption rate and extracellular acidification rate were measured by using a Seahorse XFe96 (Agilent Technologies, Santa Clara, USA) according to the manufacturer's instructions. Briefly, 12×10^3 KYSE-410 cells were seeded in an XFe96 well plate in standard cell culture medium 1 day in advance. On the day of analysis, the medium was changed to non-buffered RPMI-1640 supplemented with 10-mM glucose and 2-mM glutamine and incubated at 37°C without CO_2 for 1 hr. dichloroacetate was injected, and the cells were incubated for 15 min. Mitochondrial respiration was measured by XF Mito Stress Test Kit, and glycolysis was analysed by Glycolysis Rate Assay Kit (Agilent Technologies).

2.8 | Cell viability and apoptosis analysis

Cell viability and apoptosis were analysed by three different methods: living cell count, Annexin V-FITC binding, and cleaved PARP immunoblots. For cell count analysis, 3×10^4 cells were seeded per 12-well and incubated with the indicated amount of dichloroacetate and/or 4-MU and counted every 24 hr for 3 days. Annexin V (A13199; Invitrogen) binding to apoptotic cells was analysed at Day 3 by flow cytometry as previously described (Grandoch et al., 2009). For immunoblotting, at Day 3, cell extracts were separated by 10% SDS-PAGE and transferred to a nitrocellulose membrane by the semi-dry method. It was then incubated with 1:1,000 rabbit anti-cleaved-PARP antibody (Cell Signaling Technology Cat# v9532, RRID:AB_659884; Danvers, USA) in 2.5% BSA in TBS-T and visualized by 1:10,000 RDye 800CW Goat anti-Rabbit (926-32211; Li-COR Bioscience, Lincoln, USA). The signal intensity was quantified and normalized to mouse anti-β-tubulin (Sigma-Aldrich Cat# T7816, RRID:AB_261770) concentration.

2.9 | Quantification of O-GlcNAcylation

The amount of O-GlcNAcylated proteins was analysed by immunoblot and immunostaining. To this purpose, cells were incubated with dichloroacetate for 3 days, harvested in 2× Laemmli buffer, and proteins were separated by an 8% SDS-PAGE. After semi-dry transfer, the membrane was incubated with 1:1,000 mouse anti-O-GlcNAc

antibody (Abcam Cat# ab2739, RRID:AB_303264, Cambridge, UK) in PBS followed by 1:1,000 goat anti-mouse AlexaFluor488 (A-11029; ThermoFischer) staining. Quantified protein content was normalized to tubulin concentration. The same antibody was used for immunostaining: The cells were grown on glass slides and fixed with 4% formalin. Next, the cells were permeabilized and blocked by 10% FBS, 0.3-M glycerine, 1% BSA, and 0.1% Triton X-100 in PBS. The cells were then incubated with the O-GlcNAc antibody and Hoechst. O-GlcNAc staining was analysed by Fiji and normalized to nuclei count. The O-GlcNAc transferase inhibitor alloxan (10 mM, Sigma) was used as negative control (Konrad et al., 2002).

2.10 | Gene silencing

The 1×10^5 cells were reversely transfected with siRNA or scrambled control siRNA (Qiagen, Hilden, Germany) using lipofectamine RNAiMaxx (ThermoFisher) according to manufacturer's instructions. The following siRNAs were used (gene of interest, Qiagen order numbers): HAS3 (SI00433902, SI00433895), CD44 (SI00299705, SI03037419), RHAMM (SI02653196, SI05137384), and AllStars-Negative-Control-siRNA (SI03650318). Quantitative real-time RT-PCR was performed to confirm successful knockdown.

2.11 | 3D spheroid model

A multicellular tumour spheroid model was used to mimic three-dimensional growth: 5,000 KYSE-410 cells were planted in a round bottom 96-well BRAND microplate (Brand, Wertheim, Germany) and centrifuged for 10 min at 600× *g*. After 4-day incubation time, the spheroids were treated with 20-mM dichloroacetate and/or 300-μM 4-MU for 10 days. At Days 0, 3, 7, and 10 of treatment, pictures were taken with a Zeiss AxioObserverZ.1, and the diameter was measured using AxioVision Software (AxioVision, RRID:SCR_002677, Carl Zeiss, Oberkochen, Germany). The volume was calculated from the diameter with the formula $V = 1/6 \times \pi \times d^3$. The medium was changed at the same time points.

2.12 | Living cell toxicity assay of 3D cultures

At Day 10, spheroids were stained with either 3-μM ethidium homodimer 1 (46043; Sigma), 2-μM calcein AM (206700; Calbiochem), and 33-μM Hoechst 33342 or with 1:100 CellEvent Caspase-3/7Green Detection Reagent (C10423; Life Technologies) in combination with Hoechst as described previously (Sirenko et al., 2015). All dyes were directly added to 100-μl RPMI culture media without washing and incubated for 3 hr at 4°C.

2.13 | Immunostaining

Tumour cryosections (8 μm) were fixed with 10% formalin. Targets stained comprise 1:200 HA (HA binding protein [HAbP]), 1:200 cytokeratin 18 (CK18; guinea pig anti-CK18; GP-CK18; Progen, Heidelberg, Germany), 1:1,000 Ki67 (rabbit anti-Ki67; NB500-170; Novus, Littleton, USA), and 1:1,000 CD31 (Abcam Cat# ab7388, RRID:AB_305905). Click-it Plus TUNEL assay (C10617; ThermoFisher) was used to determine apoptotic cells according to manufacturer's instructions. Nuclei were counterstained by Hoechst. Staining was quantified by Fiji software. Five random images were selected from each tumour section and were averaged as one *n*.

2.14 | Randomization and blinding

In the in vivo experiments, the animals were randomized to either treatment group. After the tumours of the mice were harvested, the created histological slides were numbered, and the analysis was performed under blinded conditions. In vitro experiments regarding microscopic imaging were also carried out in a blinded manner. Other in vitro experiments were not conducted under blind conditions, but raw data were acquired directly from the experimental procedures and analysed through standardized procedures that reduce any possible operator bias.

2.15 | Data and statistical analysis

The data and statistical analysis comply with the recommendations of the *British Journal of Pharmacology* on experimental design and analysis in pharmacology. Statistical analysis was performed using GraphPad Prism Software 7.04 (GraphPad Prism, RRID:SCR_002798, La Jolla, USA). All results are expressed as mean ± *SD* of *n* independent experiments. Statistical comparison of two groups was performed by Student's *t* test. Three and more conditions were analysed by one-way ANOVA followed by Tukey's or Holm–Sidak's multiple comparison correction, if *F* test achieved the necessary level of statistical significance and there was no variance inhomogeneity. Statistical significance was considered at *P* values <.05.

2.16 | Materials

If not noted otherwise, all reagents and chemicals were obtained from Sigma (St. Louis, MO, USA). Dichloroacetate and 4-MU doses used for the in vitro and in vivo experiments in this study are based on studies using these compounds in monotherapy and in combination with other drugs. These studies are summarized in Tables S3–S6 (dichloroacetate in vitro studies, Table S3; dichloroacetate in vivo studies, Table S4; 4-MU in vitro studies, Table S5; and 4-MU in vivo studies, Table S6).

2.17 | Nomenclature of targets and ligands

Key protein targets and ligands in this article are hyperlinked to corresponding entries in http://www.guidetopharmacology.org, the common portal for data from the IUPHAR/BPS Guide to PHARMACOLOGY (Harding et al., 2018), and are permanently archived in the Concise Guide to PHARMACOLOGY 2017/18 (Alexander et al., 2017).

3 | RESULTS

3.1 | Treatment with dichloroacetate triggers HA matrix synthesis

In this study, we aimed at the identification of strategies that synergistically enhance the efficacy of metabolic cancer treatments. Specifically, we chose dichloroacetate as a prototypical drug as it represents the most advanced approach exploiting aerobic glycolytic metabolism in cancer cells. Oesophageal cancer was selected as a model tumour entity since it presents with a poor prognosis and few treatment options (Enzinger & Mayer, 2003); in addition, we and others identified HA in the tumour micro-environment of oesophageal squamous cancer cells as a pivotal factor of tumour progression (Lin, Karakasheva, Hicks, Bass, & Rustgi, 2016; Twarock et al., 2011).

As a premise for further investigations, we first evaluated the influence of dichloroacetate treatment on the HA matrix system. Thus, we quantified the extracellular and pericellular HA content and determined the transcriptional regulation of pivotal genes of the HA matrix system in the ESCC cell line KYSE-410 in response to dichloroacetate. In this study, we used dichloroacetate concentrations of 10, 20, and 40 mM for the cell culture experiments as this range showed a dose-dependent reduction on the cell growth of KYSE-410 cells in preliminary experiments (Figure S1) and is also found in the literature (Kankotia & Stacpoole, 2014). On the product level, we measured HA concentrations in the cell supernatant by an ELISA-like assay (Figure 1a) and pericellular HA deposition by affinity-histological stainings, both using HAbP (Figure 1b). We observed a dose-dependent increase in both assays indicating enhanced HA deposition in response to dichloroacetate treatment. Quantitative PCR analyses of the main genes of the HA matrix system consistently revealed an up-regulation of the HAS 2 and 3 (*HAS2*,*3*; Figure 1c), the hyaluronidases 1 and 2 (*HYAL1*,*2*; Figure 1d), and the HA receptors *RHAMM* and *CD44* (Figure 1e). As an up-regulated HA matrix can exhibit a strong anti-apoptotic activity, this observation might provide a basis for cellular resistance against dichloroacetate and was thus further scrutinized in the following experiments.

3.1.1 | Reconstitution of mitochondrial function by dichloroacetate activates HA synthesis via an increase in HA precursor pool and O-GlcNAcylation

In order to identify the underlying mechanism of elevated HA synthesis following dichloroacetate treatment, we first validated the effects of dichloroacetate on aerobic glycolysis (Figure 2a) and ATP production (Figure 2b). Complete curves of mitochondrial respiration and glycolytic activity are shown in Figure S2. We observed a dose-dependent decline in glycolysis accompanied by a rise in intracellular ATP levels indicating activation of mitochondria-bound OXPHOS. HPLC measurements confirmed these findings (Figure S3). Pyruvate concentrations did not significantly change under these conditions, which is compatible with a shift in pyruvate usage from lactate generation to OXPHOS (Figure S3B). In response to dichloroacetate treatment, the early glucose metabolite G6P, a key HA precursor molecule, increased in a dose-dependent manner (Figure 2C). However, FACE analysis showed that the downstream metabolite UDP-glucose, which is subsequently converted to UDP-glucuronic acid and finally integrated into the growing HA chain, did not increase with dichloroacetate stimulation (Figures 2d and S4). This finding may indicate a rapid metabolization and usage of this precursor in HA synthesis. A schematic overview of the suggested pathway is shown in Figure 3. As the second constituent of HA, GlcNAc, is synthesized by utilization of acetyl-CoA, we next investigated the effects of restored OXPHOS on GlcNAc levels and subsequent implications for HAS. Quantification of cellular acetyl-CoA levels revealed a strong dose-dependent increase in response to dichloroacetate treatment (Figure 2e) that was inhibited by the ATP citrate lyase inhibitor SB204990, which indicates its mitochondrial origin (Figure 2f). This rise in acetyl-CoA precursors also yielded a corresponding increase in cellular UDP-GlcNAc levels (Figures 2g and S4). This process was mainly accountable for the elevated HAS under dichloroacetate treatment as the inhibition of acetyl-CoA shuttling by SB204990 reversed the induction of HAS by dichloroacetate by about 75% (Figure 2h). These results indicate that the restoration of mitochondrial OXPHOS by dichloroacetate treatment causes an increase in the precursor pools of HA constituents, which provide the basis for the observed elevation of HAS. Furthermore, enhanced O-GlcNAcylation directly triggers the activity of the HAS enzymes (Tammi et al., 2011; Vigetti, Viola, Karousou, De Luca, & Passi, 2014). In line with the observed increase of the UDP-GlcNAc pool, dichloroacetate treatment resulted in a strong induction of O-GlcNAcylation of cellular proteins as determined by immunoblot (Figures 2i and S5) and immunohistochemistry (Figure 2j). This finding delineates an additional mechanism accountable for elevated HAS resulting from restored OXPHOS activity triggered by dichloroacetate.

3.1.2 | Inhibition of HA synthesis synergistically enhances apoptosis and tumour growth suppression by dichloroacetate in 2D cell culture

The OXPHOS restoring agent dichloroacetate and the HA synthesis inhibitor 4-MU both showed a suppressing effect on the growth of cultured ESCC within 3 days. However, only the combination treatment was able to decrease the cell count (Figure 4a). We used the Software CompuSyn to identify synergistic combinations of dichloroacetate and 4-MU concentrations. For the combination of a mid-range concentration of 20-mM dichloroacetate with 300-μM 4-MU, which is shown in Figure 4a, the CI value was calculated as 0.65545 denoting synergism for this combination (Table S2). Flow cytometry measurements for Annexin V^+ cells (Figure 4b) and immunoblots for PARP cleavage (Figure 4c) revealed that this effect was caused by an induction of apoptosis. In a next step, we aimed to identify the role of key parts of the HA system for mediating the synergistic enhancement of dichloroacetate by 4-MU. Therefore, we also performed growth experiments with cells that were treated with

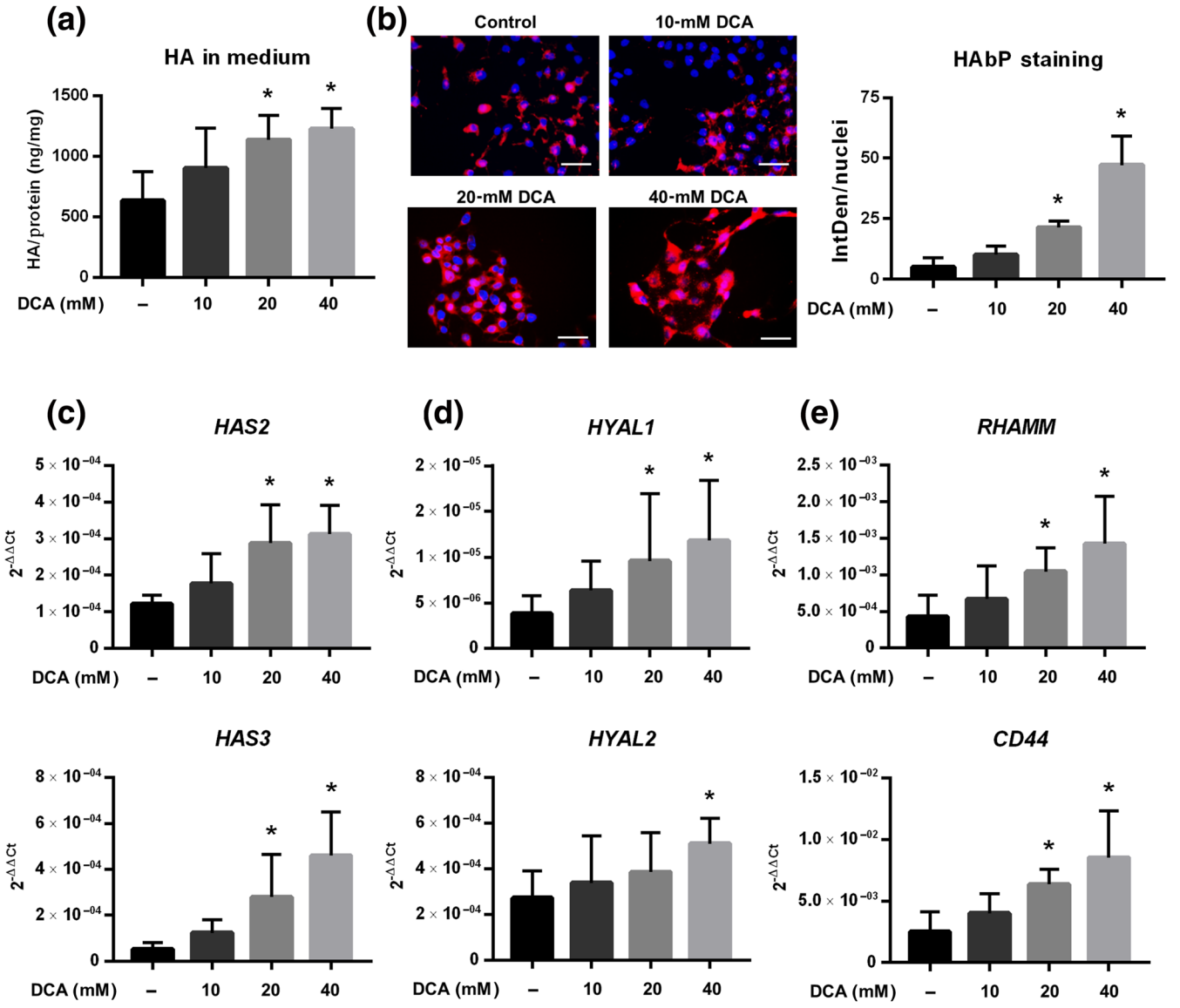

FIGURE 1 Dichloroacetate up-regulates the hyaluronan matrix in oesophageal cancer cells on the product and transcriptional levels. KYSE-410 were incubated with 10-, 20-, 40-mM dichloroacetate (DCA) for 72 hr and analysed for their hyaluronan (HA) content and expression of genes relevant to HA synthesis, degradation, and signalling. (a) HA concentration in the medium was measured by an ELISA-like immunoaffinity assay and normalized to protein content (n = 6). (b) Pericellular HA deposition (red) was stained by HA binding protein (HAbP), and its integrated density (IntDent) was normalized to nuclei (Hoechst, blue) count (n = 7, each n represents a pooled analysis of five replicates). Representative images are shown, scale bar: 100 µm. Gene expression of (c) HA synthases (*HAS2*,*3*) and (d) hyaluronidases (*HYAL1*,*2*) and (e) HA receptors *RHAMM* and *CD44* were determined and normalized to respective controls (n = 7). Data shown are means ± SD. *P < .05, significantly different from control (0-mM DCA); one-way ANOVA.

siRNAs against both HA receptors RHAMM and CD44 and HAS3, which is the main HAS isoform in the ESCC cells used in this project (Twarock et al., 2017). The knockdown of HAS3 resembled the effects of 4-MU in showing a substantial impairment of tumour cell growth that was, by trend, even more pronounced in combination with dichloroacetate. The knockdown of the HA receptors had a much weaker effect on cell growth, but this effect was strongly increased by addition of dichloroacetate (Figure 4d). These results indicate that interference with various components of the HA system, which is triggered by dichloroacetate treatment, result in a synergistic improvement of the anticancer actions of dichloroacetate.

3.2 | Combination treatment induces apoptosis and shrinkage of tumour spheroids

It has been reported that dichloroacetate shows different effectivity in vivo and in cell culture experiments (Papandreou, Goliasova, & Denko, 2011). This observation may be connected to the fact that tumour metabolism is significantly modulated by oxygen availability, which alters with the growth of the tumour. In addition, also the ECM changes in response to the spatial interaction of the embedded cells. To consider these characteristics of a developing tumour, we established a 3D tumour spheroid model to investigate the interaction

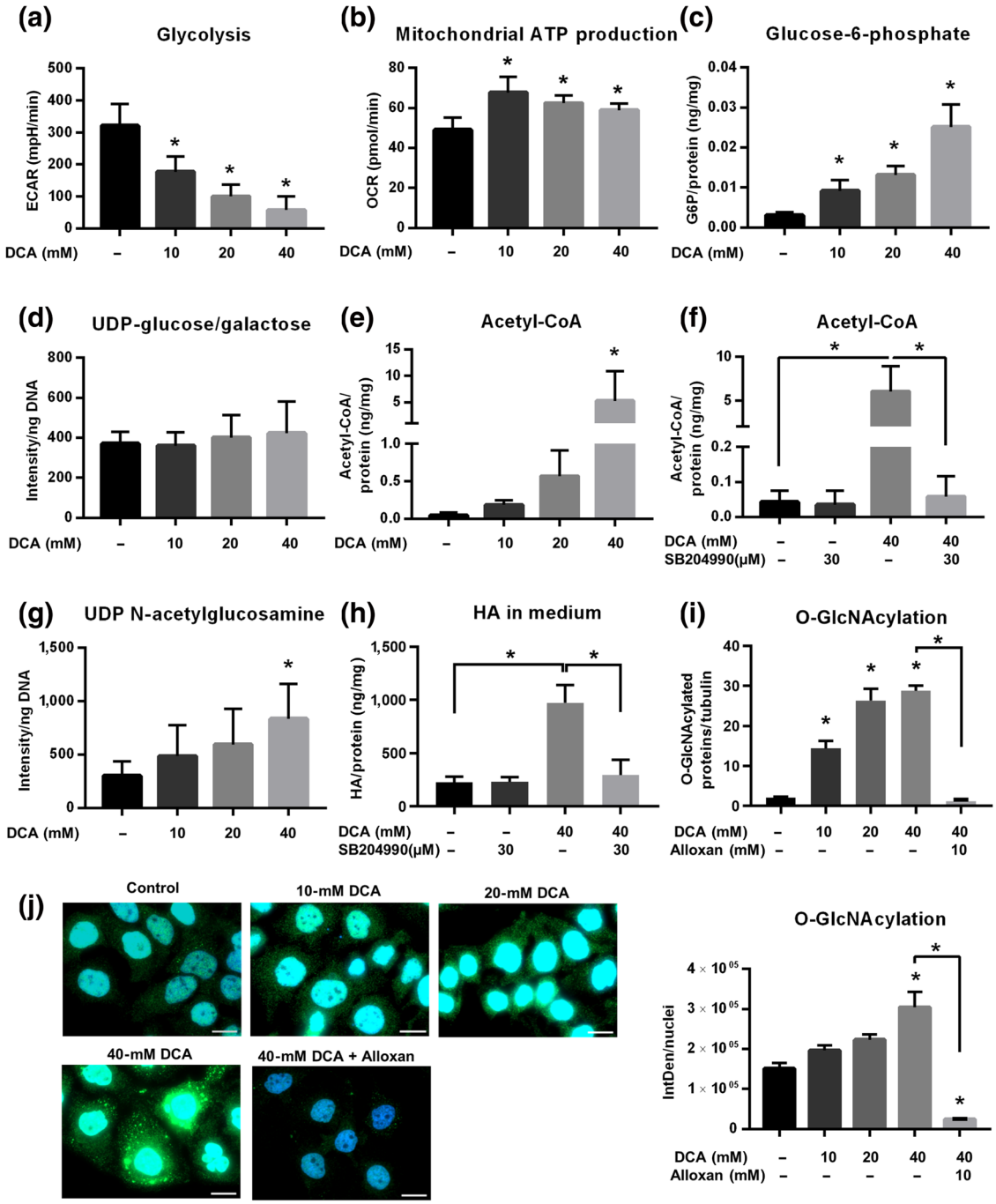

FIGURE 2 Dichloroacetate (DCA) switches the tumour cells to OXPHOS resulting in increased hyaluronan precursors and protein O-GlcNAcylation. Real-time metabolism analysis by Seahorse XFe96 with (a) Glycolysis Rate Assay Kit and (b) Mitochondrial Stress Test Kit was used to measure the acute response of KYSE-410 cells to dichloroacetate stimulation. Cells were seeded into Seahorse plates, and dichloroacetate was injected and incubated for 15 min before analysis was started. Extracellular acidification rate (ECAR) represents the amount of glycolysis, and oxygen consumption rate (OCR) defines the amount of mitochondrial respiration of 12×10^3 cells per well (each *n* represents a pooled analysis of four replicates). (c) Glucose 6-phosphate concentration was measured after dichloroacetate incubation of 3 days by colorimetric analysis. (d) The hyaluronan (HA) precursor UDP-glucose/galactose was quantified by fluorophore-assisted carbohydrate electrophoresis (FACE) and normalized to total DNA content. UDP-sugars were isolated from KYSE-410 by ENVI-Carb columns. (e) Acetyl-CoA concentration was measured by colorimetry. (f) SB204990 inhibits the export of acetyl-CoA from the mitochondria to the cytosol and was used to abolish the effects of dichloroacetate on acetyl-CoA synthesis. (g) The HA precursor *N*-acetylglucosamine was isolated and determined by FACE analysis. (h) HA concentration in the medium after inhibition of acetyl-CoA shuttling with SB204990 was measured by an ELISA-like immunoaffinity assay. GlcNAcylation of proteins was quantified by (i) western blot analysis and (j) immunostaining (O-GlcNAcylation, green; nucleus, blue). The O-GlcNAc transferase (OGT) inhibitor alloxan was used as a negative control. (a–i) $n = 6$. (j) Representative images are shown, scale bar: 20 μm ($n = 8$, each *n* represents a pooled analysis of five replicates). Data shown are means ± SD. $^*P < .05$, significantly different from control (0-mM DCA) or as indicated; one-way ANOVA.

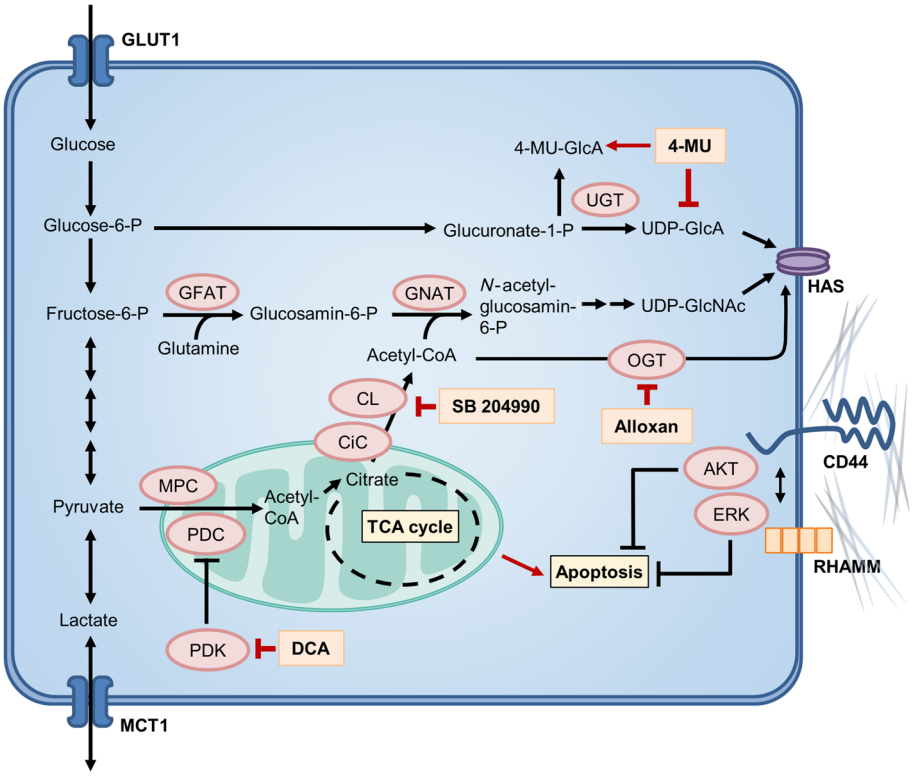

FIGURE 3 Diagram of the pathways involved in the metabolic interaction of glycolysis, mitochondrial respiration, and hyaluronan synthesis. Glucose is taken up by the glucose transporters (e.g., GLUT1) and further metabolized in the glycolysis. For energy production, pyruvate is shuttled to the mitochondria via the mitochondrial pyruvate carrier (MPC) where it is converted to acetyl-CoA by the pyruvate dehydrogenase complex (PDC), whose activity is regulated by pyruvate dehydrogenase kinase (PDK). Acetyl-CoA is then further consumed in the tricarboxylic acid cycle (TCA) to fuel ATP synthesis. In most cancer cells, this pathway is aberrant due to an up-regulation of PDK leading to an inhibition of PDC activity. This switch is characteristic for hypoxic conditions but is regularly found also in the presence of oxygen in tumour cells (Warburg effect). Under these circumstances, pyruvate is reduced to lactate, which is exported by monocarboxylate transporters (e.g., MCT1). Restoration of mitochondrial oxidative phosphorylation (OXPHOS) by the PDK inhibitor dichloroacetate (DCA) yields an increased amount of acetyl-CoA in the mitochondria, which is also shuttled to the cytosol under involvement of the citrate carrier (CiC) and the ATP-citrate lyase (CL). A reactivation of mitochondrial metabolism in tumour cells has been connected to the induction of caspase-dependent apoptosis. Our study reveals that this process also yields an increase in the hyaluronan (HA) synthesis precursors glucose 6-phosphate and *N*-acetyl-glucosamine. The latter also triggers the O-GlcNAc transferase (OGT) mediating GlcNAcylation of proteins (e.g., hyaluronan synthase [HAS]). These processes result in a pronounced increase of the extracellular matrix compound HA that inhibits apoptosis via its receptors CD44 and RHAMM. HA synthesis can be blocked by 4-methylumbelliferone (4-MU), thus providing a countermeasure for this antiapoptotic counter-regulation. GFAT, glutamine:fructose-6-phosphate aminotransferase; GNAT, acetyl-CoA:D-glucosamine *N*-acetyltransferase; UGT, UDP-glucuronyltransferase

between metabolism and ECM in this setting and to determine the effect of dichloroacetate and 4-MU during this process. Quantitative PCR analyses showed that indeed two of the major enzymes supporting the Warburg Effect, that is, PDK 1 (PDK1) and LDH A (LDHA), showed a strong transcriptional induction compared to 2D culture indicating an increase in aerobic glycolysis under these conditions. Simultaneously, also, the mRNA expression of the main HA synthase (HAS3) in the examined cells was strongly increased. This may be attributable to the demanding scaffolding needs for three-dimensional growth (Figure 5a). Given the augmented activity of both systems in this set-up, we investigated whether the combination of dichloroacetate and 4-MU is also effectively inducing apoptosis under 3D conditions. In line with our earlier findings, the combination of dichloroacetate and 4-MU resulted not only in growth inhibition, as observed with the monotherapies, but caused a pronounced decrease in spheroid volume below start size (Figure 5b). Live-Dead staining of native spheroids at Day 10 revealed that monotherapy with 4-MU (300 μM) diminished the size of the spheroid while only few dead cells were detectable. In contrast, monotherapy with dichloroacetate (20 mM) caused shedding of dead cells from the spheroid. However, only the combination of both compounds significantly reduced spheroid size and led to an extensive emergence of dead cells in and around the spheroid (Figure 5c, upper panel). This finding was corroborated by a caspase 3 staining that revealed an apoptotic core under 4-MU treatment, homogeneously distributed apoptotic cells with dichloroacetate treatment, and a widespread induction of apoptosis throughout the spheroids under the combination therapy (Figure 5c, lower panel). Silencing of RHAMM, CD44, and HAS3 basically resembled the results obtained in 2D cultures differing only in a weaker effect of the HAS3 knockdown, which may be caused by the

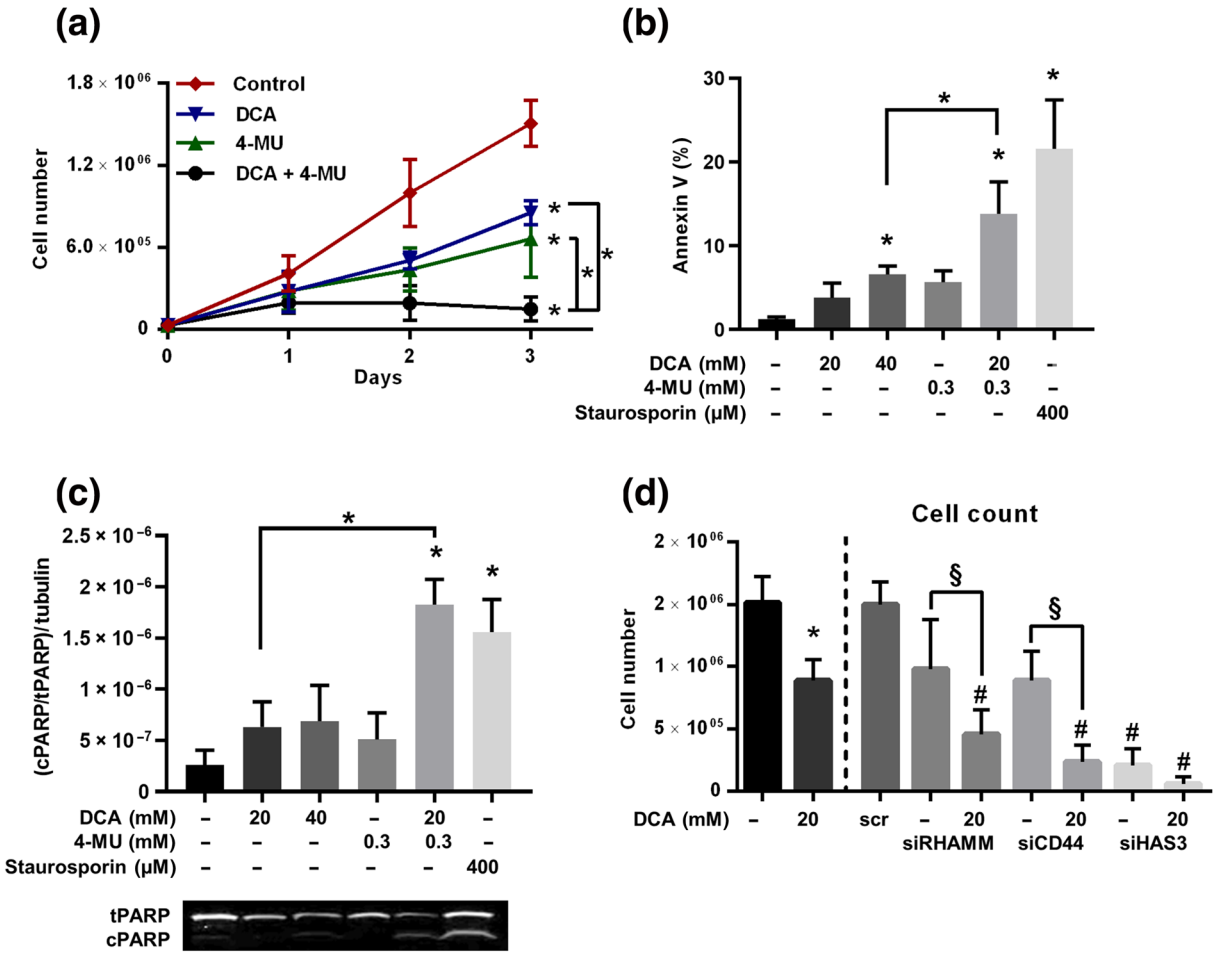

FIGURE 4 Dichloroacetate (DCA) in combination with 4-methylumbelliferone (4-MU) leads to reduced cell growth and apoptosis induction in oesophageal squamous cell carcinoma cells. (a) Cells were incubated with 20-mM dichloroacetate and/or 300-μM 4-MU and counted daily for 3 days ($n = 7$). After a 3-days of exposure to single or combination therapy, cells were collected for (b) FACS of annexin-positive cells ($n = 6$) and (c) immunoblot of cleaved PARP (cPARP). cPARP was normalized to total PARP (tPARP). A typical immunoblot for seven individual experiments is shown. Staurosporine (400 μM) was used as a positive control ($n = 7$). (d) Cell numbers were determined 3 days after gene knockdown by siRNA for hyaluronan receptors RHAMM and CD44 and hyaluronan synthase (HAS) isotype HAS3 ($n = 7$). Data shown are means ± SD. $^{*}P < .05$, significantly different from control or 0-mM DCA or as indicated; $^{\#}P < .05$, significantly different from scrambled control; $^{\S}P < .05$, significantly different from only siRNA treatment, one-way ANOVA.

strong overexpression of HAS3 in 3D culture (Figures 5, S6B, and S7A,B). The induction of cell death with dichloroacetate and 4-MU or siRHAMM, siCD44, and siHAS3 was validated by an APH assay (Figure S8A,B).

3.3 | Validation of the efficacy of the combination therapy in a nude mouse tumour xenograft regression model

To confirm our findings in vivo, we used a nude mouse tumour xenograft regression model. On Day 60, all treatments caused a significant reduction in tumour volume compared to the placebo control. However, only the combination treatment resulted in a sustained growth arrest of the tumour xenografts and in macroscopically detectable destruction of tumour tissue. In this group, the tumour volume was also significantly reduced in comparison to the monotherapies with dichloroacetate and 4-MU (Figure 6a). In line with the in vitro experiments (Figure 1a,b), histological stainings for HA (HAbP) and tumour cells (CK18) yielded an increase in HA deposition in the dichloroacetate treated group that was abolished in the 4-MU treated groups (Figure 6b). In order to detect the basis for the impeded xenograft growth in the treatment groups, we stained the tumour sections for the proliferation marker Ki67 (Figure 6c) and the endothelial cell marker CD31 (Figure 6d). Proliferating cells were diminished most in response to the combination treatment while the monotherapies also decreased the number of proliferating cells. Only dichloroacetate and dichloroacetate/4-MU resulted in a significant reduction of CD31 positive vessels. However, also, 4-MU treatment showed a similar tendency. Apoptotic cells were visualized by TUNEL staining (Figure 6e). Intriguingly, only the

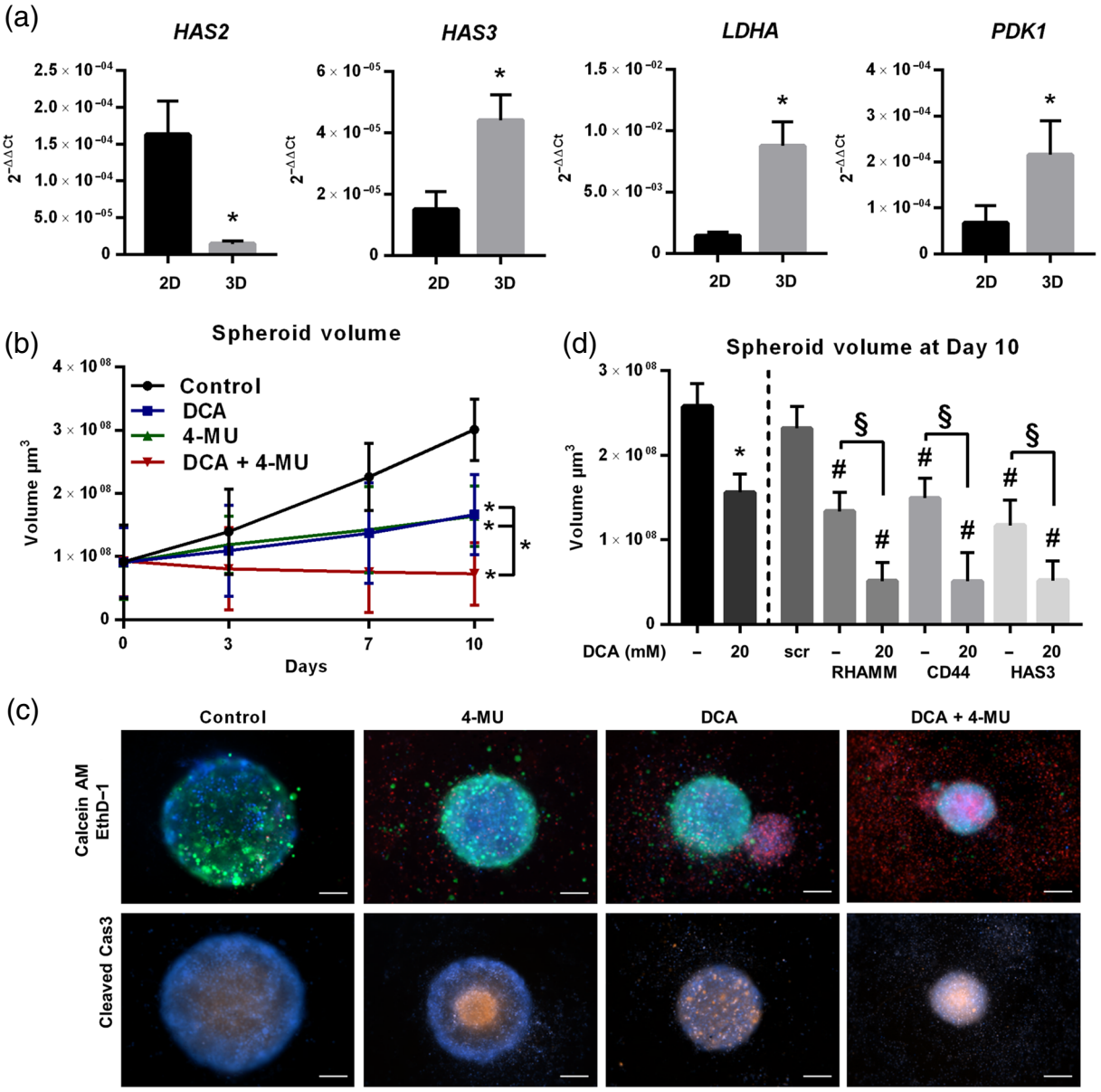

FIGURE 5 Combination of dichloroacetate (DCA) and 4-methylumbelliferone (4-MU) causes reduction in tumour spheroid volumes and induction of apoptosis. (a) Comparison of the gene expression between 2D and 3D cultures of the most relevant components of the hyaluronan system and aerobic glycolysis (n = 6, each n represents a pooled analysis of eight replicates). (b) Spheroid volumes of 24 replicate spheroids per condition were measured. 3D cultures were grown for 4 days until incubation with drugs (20-mM dichloroacetate, 300-µM 4-MU, or the combination of both) was started. The volume was measured over a 10-day period and observed by light microscopy. The volume of a sphere was calculated based on the diameter with the formula $V = 1/6 \times \pi \times d^3$ (n = 6). (c) At Day 10, spheroids were stained for living (calcein AM, green) and dead (ethidium homodimer 1 [EthD-1], red) cells or for cleaved caspase 3 (Cas3, orange). Nuclei were counterstained with Hoechst (blue). Representative images are shown, scale bar: 200 µm. (d) siRNA knockdown of RHAMM, CD44, and HAS3 was performed prior to spheroid formation. Additional stimulation with 20-mM dichloroacetate was performed at Day 4. The experiments were followed for 10 d. Scrambled siRNA was used to exclude adverse effects of siRNA incorporation (n = 6; one n included 24 spheroids per condition). Data shown are means ± SD. $^{*}P < .05$, significantly different from 2D values or as indicated; $^{\#}P < .05$ significantly different from scrambled control; $^{\S}P < .05$, significantly different from only siRNA treatment; one-way ANOVA,

combination treatment caused a pronounced increase in apoptotic cells. The therapy was well tolerated in all treatment groups. Taken together, these experiments show that the combination of dichloroacetate and 4-MU may be a safe and effective treatment option for oesophageal cancer in vivo.

4 | DISCUSSION

This study provided a deeper insight into the close connection between tumour metabolism and ECM regulation. It demonstrated that reconstitution of mitochondrial OXPHOS and subsequent

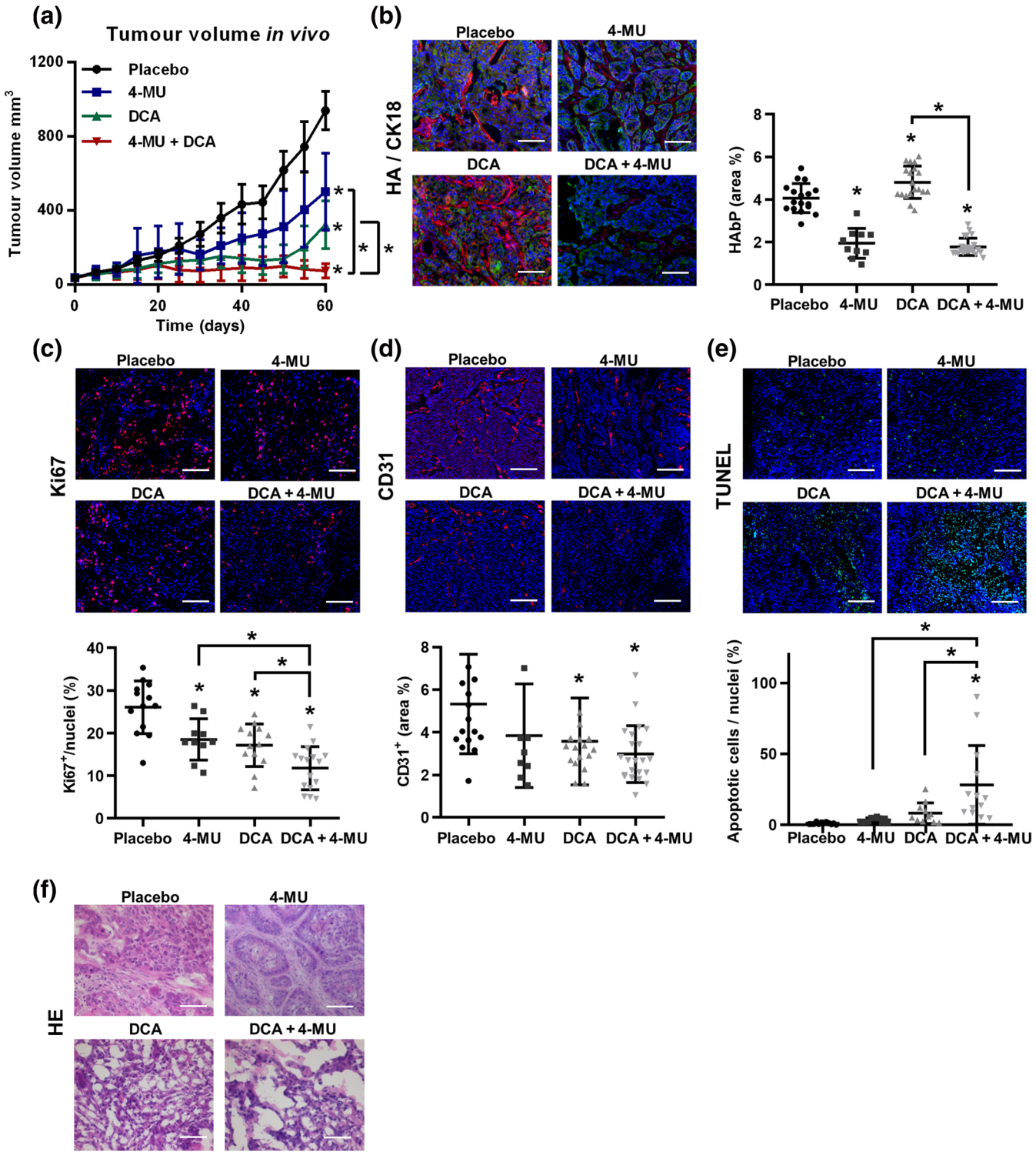

FIGURE 6 The combination of dichloroacetate (DCA) and 4-methylumbelliferone (4-MU) reduces tumour growth and proliferation and induces hyaluronan (HA) synthesis and apoptosis in vivo. (a) Treatment with the testing substances started after a tumour volume of >30 mm^3 was detected. Tumour growth was measured by calipers and observed throughout 60 days. Placebo n = 15, 4-MU n = 9, dichloroacetate n = 10, dichloroacetate + 4-MU n = 13. Residual tumours were retrieved, and cryosections were drawn. The slides were stained for (b) HA deposition (HA binding protein [HAbP], red) in the tumour (CK18, green) and stroma, (c) proliferative activity of tumour cells (Ki67, red), and (d) vessels (CD31, red). (e) TUNEL staining (green) was used to measure the amount of apoptosis that is induced by single or combinational treatment. (f) HE staining of tumour tissues was used to evaluate the morphology of tumour and stroma. Representative images are shown, scale bars: (b–e) 100 μm, (f) 50 μm. Data shown are individual values, with means ± SD. *P < .05, significantly different from placebo or as indicated; one-way ANOVA.

changes in the cellular glucose flux were metabolically coupled to the antiapoptotic HA system. This observation presents a new mechanism for resistance to metabolic anticancer therapies targeting the Warburg effect. This process may be further aggravated by the strong transcriptional activation of both aerobic glycolysis and HAS under three-dimensional growth, as observed in this study. To overcome this metabolic counter-regulation, we tested pharmacological inhibition of the HA matrix synthesis by the low MW compound 4-MU in combination with dichloroacetate treatment, which indeed caused increased apoptosis, eventually leading to synergistically enhanced anti-tumour effects in vitro and in vivo.

In detail, we describe two mechanisms that increase the HA synthesis when mitochondrial OXPHOS is restored by dichloroacetate. First, the G6P precursor pool is increased, thus providing more fuel for the synthesis of UDP-glucuronic acid, one of the two substrates for HA synthesis used by the HAS enzymes. This is in line with earlier reports in muscle cells showing that dichloroacetate inhibits glycolysis by an unknown mechanism resulting in an increase of G6P in this cell type (Clark et al., 1987). This observation may be explained by the inhibition of phosphofructokinase II via O-GlcNAcylation and is further discussed below. Second, activation of the PDC yielded a pronounced increase in mitochondrial acetyl-CoA that fuels OXPHOS but is also shuttled to the cytosol, where it serves as a cofactor for the synthesis of GlcNAc, which is the second substrate for HA synthesis.

In this context, it is noteworthy that HA is exclusively synthesized from these two early glucose metabolites. Accordingly, substrate availability directly correlates with the extent of HA synthesis (Tammi et al., 2011). For instance, UDP-sugar accumulation has been shown to enhance HA synthesis in breast cancer (Oikari et al., 2018). Interestingly, the synthesis of other glycosaminoglycans is modulated by UDP-GlcNAc availability, thus extending the effect of our findings beyond regulation of HA synthesis (Vigetti et al., 2012). One remarkable observation in our experiments is that we detected a rise in G6P and UDP-GlcNAc levels under dichloroacetate treatment but no increase in UDP-glucuronic acid. This may be caused by a rapid use of this immediate precursor for HA synthesis due to a high activity of the HAS enzymes triggered by the mechanisms discussed below.

In addition to providing fuel for HA synthesis, UDP-GlcNAc also holds the potential to induce HA synthesis by post-translational mechanisms (Moretto et al., 2015): UDP-GlcNAc concentrations control the activity of the O-GlcNAc transferase and thereby the O-GlcNAcylation of various proteins including the HAS enzymes. Indeed, a great extent of O-GlcNAcylation in breast cancer cells was found to correlate with the levels of HAS enzymes, accumulation of HA, and poor outcome (Tiainen et al., 2016). Specifically for HAS3, the predominant isoform in the ESCC cell line used in our study, it has been reported that cytosolic levels of UDP-GlcUA and UDP-GlcNAc regulate its activity by orchestrating the shuttling of this isoform from Golgi to the plasma membrane and facilitating its O-GlcNAcylation in melanoma cells (Deen et al., 2016). However, this study is the first to describe a connection between mitochondrial acetyl-CoA synthesis, UDP-GlcNAc levels, and HA matrix augmentation. To prove the link of mitochondrial activity and increased cytosolic GlcNAc levels, we used the ATP citrate-lyase inhibitor SB-204990, which inhibits the cytosolic conversion of citrate to acetyl-CoA, thus prohibiting the shuttling of acetyl-CoA from mitochondria to the cytosol (Pearce et al., 1998). This experiment shows that mitochondria-dependent acetyl-CoA synthesis is an important step for the induction of HA synthesis via increased GlcNAc concentration under restored Krebs cycle activity.

Recently, these and other roles of O-GlcNAcylation as a nutrient-dependent regulator of cell functions have been summarised in a comprehensive review (Hart, 2019). The concentration of UDP-GlcNAc is a highly responsive sensor for the availability and flux of nutrients through major metabolic pathways and the activity of hexosamine biosynthesis. Thus, O-GlcNAcylation orchestrates a wide range of cellular processes in response to glycolytic activity including regulation of gene expression and methylation, cell cycle, cytokinesis, and the cytoskeleton. It is induced by cellular stress and mediates protection against cellular damage, by regulating DNA repair mechanisms, for instance. Moreover, O-GlcNAcylation is also an important factor connecting metabolism to epigenetic regulation (Hanover, Krause, & Love, 2012). Of note, O-GlcNAcylation and phosphorylation show a mutually exclusive interplay in protein activation and also exhibit a feedback crosstalk between the involved regulating enzymes. Prolonged elevation of O-GlcNAcylation promotes several age-associated chronic diseases, that is, diabetes, neurodegenerative diseases, and cancer. O-GlcNAcylation was also shown to inhibit phosphofructokinase II, thus increasing the flux of glucose metabolites into the pentose phosphate pathway (Yi et al., 2012). As the precursors of HA, G6P and fructose 6-phosphate, originate from earlier steps in glycolysis, this observation may explain the elevated G6P levels in response to dichloroacetate treatment. Aberrations in O-GlcNAc cycling enzymes are considered as a new characteristic of cancer and have been connected to the metabolic reprogramming in cancer cells and may represent a novel therapeutic target (Fardini, Dehennaut, Lefebvre, & Issad, 2013). As elevated O-GlcNAcylation has been reported in many cancer entities (Slawson & Hart, 2011), the increase of this process by dichloroacetate, which we report here, should be further explored in further studies to determine whether this may represent a negative dichloroacetate side effect, independent of HA elevation.

In addition to the effects of our findings on tumour cells, the induction of HA and GlcNAc levels by dichloroacetate may also contribute to its restorative effects on cellular stress, by regulation of cellular homeostasis. For instance, dichloroacetate has been proposed as a metabolic therapy for myocardial ischaemia and failure by facilitating aerobic oxidation of carbohydrates of fatty acids (Bersin & Stacpoole, 1997), a concept that has been assessed in several studies. These protective effects may be also dependent on increased O-GlcNAcylation, as discussed above, or on increased HA synthesis, as this process has been linked to inhibition of apoptosis. In support of this thesis, HA was recently found to promote healing after ischaemia-reperfusion injury (Petz et al., 2019). These considerations could also apply to other conditions such as septic shock (McCall et al., 2018), diabetes mellitus, and hyperlipoproteinaemia (Stacpoole et al., 1978), as well as

pulmonary arterial hypertension and other diseases (James et al., 2017). Thus, the mechanisms elucidated in our study may also have long-term consequences on cellular processes beyond HA matrix regulation.

In addition to the observed metabolic stimulation of HA synthesis via an elevated supply of precursors and post-translational activation by GlcNAcylation, transcriptional changes were also involved in increasing HA synthesis following dichloroacetate treatment. We detected a strong dose-dependent up-regulation of the vital genes involved in HAS (HAS2-3), catabolism (HYAL1,2), and signalling (CD44, RHAMM). This effect may either be attributable to a positive transcriptional feedback loop that has been described (Tammi et al., 2011) or to a direct influence of the metabolic changes under dichloroacetate treatment on the respective gene promoters. Little is known about metabolic effects on HAS transcription but, in human smooth muscle cells, a drop in energy homeostasis causes a decline in HAS2 expression via **AMP kinase** (Vigetti et al., 2011).

This study also provides an explanation for the paradoxical observation that dichloroacetate was more active in vivo than in vitro in some experimental setups (Papandreou et al., 2011). The comparison of 2D and 3D cell cultures showed strong up-regulation of PDK1 and LDHA when grown as spheroids indicating that these systems are more active in this model, which better correlates to in vivo growth. This observation is in line with the fact that multicellular tumour spheroids are thought to be a better model for the hypoxia found in solid tumours, a condition that is linked to activation of aerobic glycolysis (Riffle & Hegde, 2017). In addition, we show for the first time that three-dimensional growth also causes strong transcriptional induction of HAS3. This may be the result of increased scaffolding needs but is likely also to present an important survival factor in advanced carcinogenesis. Indeed, only the targeting of both systems with the combination of dichloroacetate and 4-MU caused shrinkage of the tumour spheroids below their initial size. Our data suggest that the induction of the antiapoptotic HA matrix may be intrinsic to the mechanism of action of drugs that restore OXPHOS in cancer cells.

In our study, we first characterized a counter-regulatory mechanism involving a metabolic link between OXPHOS and elevated synthesis of the ECM compound HA. In a next step, we specifically targeted this rescue mechanism by abolishing the activity of the antiapoptotic HA system, which yielded a pronounced synergistic action of dichloroacetate and 4-MU. In contrast to most of the published studies on dichloroacetate combination therapies, we used a tumour xenograft regression model, which reflects the clinical situation more appropriately in that treatment starts after a defined tumour volume is detected. Of note, also under this condition, we found a sustained inhibition of tumour growth with a marked induction of apoptosis in the tumour tissue.

A limitation of this study is that our results have been produced using one tumour cell line. However, as summarized in Tables S3 and S4, the effects of dichloroacetate on mitochondria reactivation and subsequent tumour growth inhibition have been shown in a wide variety of tumour models in vitro and in vivo. As restored mitochondrial activity is most likely to result in elevated acetyl-CoA production in general, we propose that the mechanism described here may also be valid for other cell types. Given that 4-MU was also reported to inhibit HAS, and consequently tumour growth, in a wide variety of tumour cells types (as summarised in Tables S5 and S6), it can be assumed that it would exhibit the same synergism with dichloroacetate as reported here in other cell types. Nevertheless, this assumption should be tested with other tumour entities and in other models.

This study shows that the metabolic changes induced by reactivation of mitochondrial OXPHOS result in a pronounced activation of HA matrix generation by an increase of the HA precursor pool and O-GlcNAcylation, which in turn supports the survival of the tumour cells. This process can be inhibited by the orally available HAS inhibitor 4-MU, which yielded strong synergistic actions with dichloroacetate in vitro and in vivo. As the resistance mechanism described in this study is likely to be inherent in therapies targeting the Warburg effect, 4-MU may also be a promising synergistic partner for these metabolic anticancer therapies as well. As 4-MU is approved for human use in many countries, the results of this study should be applicable to new clinical studies testing the therapeutic value of this combination for metabolic anticancer therapy. These findings provide the basis for further research on the effects of tumour metabolism on the tumour micro-environment and for testing this combination in clinical studies.

ACKNOWLEDGEMENT

This work was supported by the Forschungskommission der Heinrich-Heine-Universität Düsseldorf (Grant 51/2015).

AUTHOR CONTRIBUTIONS

S.T. designed the experiments, researched and interpreted data, and wrote the manuscript. C.R. researched and interpreted data and wrote parts of the manuscript. K.B., O.R., I.K., D.G, K.G., and M.G. researched data and reviewed the manuscript. J.W.F. designed the experiments, contributed guidance, and reviewed the manuscript.

CONFLICT OF INTEREST

The authors declare no conflicts of interest.

DECLARATION OF TRANSPARENCY AND SCIENTIFIC RIGOUR

This Declaration acknowledges that this paper adheres to the principles for transparent reporting and scientific rigour of preclinical research as stated in the *BJP* guidelines for Design & Analysis, Immunoblotting and Immunochemistry, and Animal Experimentation, and as recommended by funding agencies, publishers and other organisations engaged with supporting research.

DATA AVAILABILITY STATEMENT

All data generated or analysed during this study are included in this published article and its supplementary information files.

ORCID

Sören Twarock https://orcid.org/0000-0001-9252-1353

REFERENCES

Alexander, S. P. H., Fabbro, D., Kelly, E., Marrion, N. V., Peters, J. A., Faccenda, E., … Collaborators, C. G. T. P. (2017). THE CONCISE GUIDE TO PHARMACOLOGY 2017/18: Enzymes. *British Journal of Pharmacology*, *174*, S272–S359. https://doi.org/10.1111/bph.13877

Bersin, R. M., & Stacpoole, P. W. (1997). Dichloroacetate as metabolic therapy for myocardial ischemia and failure. *American Heart Journal*, *134*, 841–855. https://doi.org/10.1016/S0002-8703(97)80007-5

Bonnet, S., Archer, S. L., Allalunis-Turner, J., Haromy, A., Beaulieu, C., Thompson, R., … Michelakis, E. D. (2007). A mitochondria-K+ channel axis is suppressed in cancer and its normalization promotes apoptosis and inhibits cancer growth. *Cancer Cell*, *11*, 37–51. https://doi.org/10.1016/j.ccr.2006.10.020

Chanmee, T., Ontong, P., & Itano, N. (2016). Hyaluronan: A modulator of the tumor microenvironment. *Cancer Letters*, *375*, 20–30. https://doi.org/10.1016/j.canlet.2016.02.031

Chen, L., & Bourguignon, L. Y. (2014). Hyaluronan-CD44 interaction promotes c-Jun signaling and miRNA21 expression leading to Bcl-2 expression and chemoresistance in breast cancer cells. *Molecular Cancer*, *13*, 52. https://doi.org/10.1186/1476-4598-13-52

Chu, Q. S., Sangha, R., Spratlin, J., Vos, L. J., Mackey, J. R., McEwan, A. J., … Michelakis, E. D. (2015). A phase I open-labeled, single-arm, dose-escalation, study of dichloroacetate (DCA) in patients with advanced solid tumors. *Investigational New Drugs*, *33*, 603–610. https://doi.org/10.1007/s10637-015-0221-y

Clark, A. S., Mitch, W. E., Goodman, M. N., Fagan, J. M., Goheer, M. A., & Curnow, R. T. (1987). Dichloroacetate inhibits glycolysis and augments insulin-stimulated glycogen synthesis in rat muscle. *The Journal of Clinical Investigation*, *79*, 588–594. https://doi.org/10.1172/JCI112851

Deen, A. J., Arasu, U. T., Pasonen-Seppanen, S., Hassinen, A., Takabe, P., Wojciechowski, S., … Oikari, S. (2016). UDP-sugar substrates of HAS3 regulate its O-GlcNAcylation, intracellular traffic, extracellular shedding and correlate with melanoma progression. *Cellular and Molecular Life Sciences*, *73*, 3183–3204. https://doi.org/10.1007/s00018-016-2158-5

Dunbar, E. M., Coats, B. S., Shroads, A. L., Langaee, T., Lew, A., Forder, J. R., … Stacpoole, P. W. (2014). Phase 1 trial of dichloroacetate (DCA) in adults with recurrent malignant brain tumors. *Investigational New Drugs*, *32*, 452–464. https://doi.org/10.1007/s10637-013-0047-4

Enzinger, P. C., & Mayer, R. J. (2003). Esophageal cancer. *The New England Journal of Medicine*, *349*, 2241–2252. https://doi.org/10.1056/NEJMra035010

Fardini, Y., Dehennaut, V., Lefebvre, T., & Issad, T. (2013). O-GlcNAcylation: A new cancer hallmark? *Frontiers in Endocrinology*, *4*, 99.

Garon, E. B., Christofk, H. R., Hosmer, W., Britten, C. D., Bahng, A., Crabtree, M. J., … Slamon, D. J. (2014). Dichloroacetate should be considered with platinum-based chemotherapy in hypoxic tumors rather than as a single agent in advanced non-small cell lung cancer. *Journal of Cancer Research and Clinical Oncology*, *140*, 443–452. https://doi.org/10.1007/s00432-014-1583-9

Grandoch, M., Bujok, V., Fleckenstein, D., Schmidt, M., Fischer, J. W., & Weber, A. A. (2009). Epac inhibits apoptosis of human leukocytes. *Journal of Leukocyte Biology*, *86*, 847–849. https://doi.org/10.1189/jlb.0109048

Hanover, J. A., Krause, M. W., & Love, D. C. (2012). Bittersweet memories: Linking metabolism to epigenetics through O-GlcNAcylation. *Nature Reviews. Molecular Cell Biology*, *13*, 312–321. https://doi.org/10.1038/nrm3334

Harding, S. D., Sharman, J. L., Faccenda, E., Southan, C., Pawson, A. J., Ireland, S., … NC-IUPHAR (2018). The IUPHAR/BPS guide to pharmacology in 2018: Updates and expansion to encompass the new guide to immunopharmacology. *Nucleic Acids Research*, *46*, D1091–D1106. https://doi.org/10.1093/nar/gkx1121

Hart, G. W. (2019). Nutrient regulation of signaling and transcription. *The Journal of Biological Chemistry*, *294*, 2211–2231. https://doi.org/10.1074/jbc.AW119.003226

Ishiguro, T., Ishiguro, M., Ishiguro, R., & Iwai, S. (2012). Cotreatment with dichloroacetate and omeprazole exhibits a synergistic antiproliferative effect on malignant tumors. *Oncology Letters*, *3*, 726–728. https://doi.org/10.3892/ol.2012.552

Itano, N., Sawai, T., Yoshida, M., Lenas, P., Yamada, Y., Imagawa, M., … Kimata, K. (1999). Three isoforms of mammalian hyaluronan synthases have distinct enzymatic properties. *The Journal of Biological Chemistry*, *274*, 25085–25092. https://doi.org/10.1074/jbc.274.35.25085

James, M. O., Jahn, S. C., Zhong, G., Smeltz, M. G., Hu, Z., & Stacpoole, P. W. (2017). Therapeutic applications of dichloroacetate and the role of glutathione transferase zeta-1. *Pharmacology & Therapeutics*, *170*, 166–180. https://doi.org/10.1016/j.pharmthera.2016.10.018

Kakizaki, I., Kojima, K., Takagaki, K., Endo, M., Kannagi, R., Ito, M., … Itano, N. (2004). A novel mechanism for the inhibition of hyaluronan biosynthesis by 4-methylumbelliferone. *The Journal of Biological Chemistry*, *279*, 33281–33289. https://doi.org/10.1074/jbc.M405918200

Kankotia, S., & Stacpoole, P. W. (2014). Dichloroacetate and cancer: New home for an orphan drug? *Biochimica et Biophysica Acta*, *1846*, 617–629. https://doi.org/10.1016/j.bbcan.2014.08.005

Kaufmann, P., Engelstad, K., Wei, Y., Jhung, S., Sano, M. C., Shungu, D. C., … de Vivo, D. C. (2006). Dichloroacetate causes toxic neuropathy in MELAS: A randomized, controlled clinical trial. *Neurology*, *66*, 324–330. https://doi.org/10.1212/01.wnl.0000196641.05913.27

Kilkenny, C., Browne, W., Cuthill, I. C., Emerson, M., & Altman, D. G. (2010). Animal research: Reporting *in vivo* experiments: The ARRIVE guidelines. *British Journal of Pharmacology*, *160*, 1577–1579.

Konrad, R. J., Zhang, F., Hale, J. E., Knierman, M. D., Becker, G. W., & Kudlow, J. E. (2002). Alloxan is an inhibitor of the enzyme O-linked *N*-acetylglucosamine transferase. *Biochemical and Biophysical Research Communications*, *293*, 207–212. https://doi.org/10.1016/S0006-291X(02)00200-0

Lin, E. W., Karakasheva, T. A., Hicks, P. D., Bass, A. J., & Rustgi, A. K. (2016). The tumor microenvironment in esophageal cancer. *Oncogene*, *35*, 5337–5349. https://doi.org/10.1038/onc.2016.34

Lokeshwar, V. B., Lopez, L. E., Munoz, D., Chi, A., Shirodkar, S. P., Lokeshwar, S. D., … Altman, N. (2010). Antitumor activity of hyaluronic acid synthesis inhibitor 4-methylumbelliferone in prostate cancer cells. *Cancer Research*, *70*, 2613–2623. https://doi.org/10.1158/0008-5472.CAN-09-3185

Martinez-Outschoorn, U. E., Peiris-Pages, M., Pestell, R. G., Sotgia, F., & Lisanti, M. P. (2017). Cancer metabolism: A therapeutic perspective. *Nature Reviews. Clinical Oncology*, *14*, 11–31. https://doi.org/10.1038/nrclinonc.2016.60

McCall, C. E., Zabalawi, M., Liu, T., Martin, A., Long, D. L., Buechler, N. L., … Vachharajani, V. (2018). Pyruvate dehydrogenase complex stimulation promotes immunometabolic homeostasis and sepsis survival. *JCI Insight*, *3*. https://doi.org/10.1172/jci.insight.99292

McGrath, J. C., & Lilley, E. (2015). Implementing guidelines on reporting research using animals (ARRIVE etc.): New requirements for publication in *BJP*. *British Journal of Pharmacology*, *172*, 3189–3193. https://doi.org/10.1111/bph.12955

Michelakis, E. D., Sutendra, G., Dromparis, P., Webster, L., Haromy, A., Niven, E., … Petruk, K. C. (2010). Metabolic modulation of glioblastoma with dichloroacetate. *Science Translational Medicine*, *2*, 31ra34.

Michelakis, E. D., Webster, L., & Mackey, J. R. (2008). Dichloroacetate (DCA) as a potential metabolic-targeting therapy for cancer. *British Journal of Cancer*, *99*, 989–994. https://doi.org/10.1038/sj.bjc.6604554

Misra, S., Hascall, V. C., Markwald, R. R., & Ghatak, S. (2015). Interactions between hyaluronan and its receptors (CD44, RHAMM) regulate the activities of inflammation and cancer. *Frontiers in Immunology*, *6*, 201.

Morera, D. S., Hennig, M. S., Talukder, A., Lokeshwar, S. D., Wang, J., Garcia-Roig, M., … Lokeshwar, V. B. (2017). Hyaluronic acid family in bladder cancer: Potential prognostic biomarkers and therapeutic targets. *British Journal of Cancer*, *117*, 1507–1517. https://doi.org/10.1038/bjc.2017.318

Moretto, P., Karousou, E., Viola, M., Caon, I., D'Angelo, M. L., De Luca, G., … Vigetti, D. (2015). Regulation of hyaluronan synthesis in vascular diseases and diabetes. *Journal Diabetes Research*, *2015*, 167283.

Nagy, N., Freudenberger, T., Melchior-Becker, A., Rock, K., Ter Braak, M., Jastrow, H., … Fischer, J. W. (2010). Inhibition of hyaluronan synthesis accelerates murine atherosclerosis: Novel insights into the role of hyaluronan synthesis. *Circulation*, *122*, 2313–2322. https://doi.org/10.1161/CIRCULATIONAHA.110.972653

Nakazawa, H., Yoshihara, S., Kudo, D., Morohashi, H., Kakizaki, I., Kon, A., … Sasaki, M. (2006). 4-Methylumbelliferone, a hyaluronan synthase suppressor, enhances the anticancer activity of gemcitabine in human pancreatic cancer cells. *Cancer Chemotherapy and Pharmacology*, *57*, 165–170. https://doi.org/10.1007/s00280-005-0016-5

Ohashi, T., Akazawa, T., Aoki, M., Kuze, B., Mizuta, K., Ito, Y., & Inoue, N. (2013). Dichloroacetate improves immune dysfunction caused by tumor-secreted lactic acid and increases antitumor immunoreactivity. *International Journal of Cancer Journal International du Cancer*, *133*, 1107–1118. https://doi.org/10.1002/ijc.28114

Oikari, S., Kettunen, T., Tiainen, S., Hayrinen, J., Masarwah, A., Sudah, M., … Auvinen, P. (2018). UDP-sugar accumulation drives hyaluronan synthesis in breast cancer. *Matrix Biology*, *67*, 63–74. https://doi.org/10.1016/j.matbio.2017.12.015

Palyi-Krekk, Z., Barok, M., Isola, J., Tammi, M., Szollosi, J., & Nagy, P. (2007). Hyaluronan-induced masking of ErbB2 and CD44-enhanced trastuzumab internalisation in trastuzumab resistant breast cancer. *European Journal of Cancer*, *43*, 2423–2433. https://doi.org/10.1016/j.ejca.2007.08.018

Papandreou, I., Goliasova, T., & Denko, N. C. (2011). Anticancer drugs that target metabolism: Is dichloroacetate the new paradigm? *International Journal of Cancer Journal International du Cancer*, *128*, 1001–1008. https://doi.org/10.1002/ijc.25728

Pearce, N. J., Yates, J. W., Berkhout, T. A., Jackson, B., Tew, D., Boyd, H., … Groot, P. H. (1998). The role of ATP citrate-lyase in the metabolic regulation of plasma lipids. Hypolipidaemic effects of SB-204990, a lactone prodrug of the potent ATP citrate-lyase inhibitor SB-201076. *The Biochemical Journal*, *334*(Pt 1), 113–119. https://doi.org/10.1042/bj3340113

Petz, A., Grandoch, M., Gorski, D. J., Abrams, M., Piroth, M., Schneckmann, R., … Fischer, J. W. (2019). Cardiac hyaluronan synthesis is critically involved in the cardiac macrophage response and promotes healing after ischemia reperfusion injury. *Circulation Research*, *124*, 1433–1447. https://doi.org/10.1161/CIRCRESAHA.118.313285

Piccioni, F., Fiore, E., Bayo, J., Atorrasagasti, C., Peixoto, E., Rizzo, M., … Mazzolini, G. (2015). 4-Methylumbelliferone inhibits hepatocellular carcinoma growth by decreasing IL-6 production and angiogenesis. *Glycobiology*, *25*, 825–835. https://doi.org/10.1093/glycob/cwv023

Pickup, M. W., Mouw, J. K., & Weaver, V. M. (2014). The extracellular matrix modulates the hallmarks of cancer. *EMBO Reports*, *15*, 1243–1253. https://doi.org/10.15252/embr.201439246

Riffle, S., & Hegde, R. S. (2017). Modeling tumor cell adaptations to hypoxia in multicellular tumor spheroids. *Journal of Experimental & Clinical Cancer Research*, *36*, 102. https://doi.org/10.1186/s13046-017-0570-9

Schindelin, J., Arganda-Carreras, I., Frise, E., Kaynig, V., Longair, M., Pietzsch, T., … Cardona, A. (2012). Fiji: An open-source platform for biological-image analysis. *Nature Methods*, *9*, 676–682. https://doi.org/10.1038/nmeth.2019

Sirenko, O., Mitlo, T., Hesley, J., Luke, S., Owens, W., & Cromwell, E. F. (2015). High-content assays for characterizing the viability and morphology of 3D cancer spheroid cultures. *Assay and Drug Development Technologies*, *13*, 402–414. https://doi.org/10.1089/adt.2015.655

Slawson, C., & Hart, G. W. (2011). O-GlcNAc signalling: Implications for cancer cell biology. *Nature Reviews Cancer*, *11*, 678–684. https://doi.org/10.1038/nrc3114

Stacpoole, P. W., Kerr, D. S., Barnes, C., Bunch, S. T., Carney, P. R., Fennell, E. M., … Valenstein, E. (2006). Controlled clinical trial of dichloroacetate for treatment of congenital lactic acidosis in children. *Pediatrics*, *117*, 1519–1531. https://doi.org/10.1542/peds.2005-1226

Stacpoole, P. W., Kurtz, T. L., Han, Z., & Langaee, T. (2008). Role of dichloroacetate in the treatment of genetic mitochondrial diseases. *Advanced Drug Delivery Reviews*, *60*, 1478–1487. https://doi.org/10.1016/j.addr.2008.02.014

Stacpoole, P. W., Moore, G. W., & Kornhauser, D. M. (1978). Metabolic effects of dichloroacetate in patients with diabetes mellitus and hyperlipoproteinemia. *The New England Journal of Medicine*, *298*, 526–530. https://doi.org/10.1056/NEJM197803092981002

Sun, R. C., Board, P. G., & Blackburn, A. C. (2011). Targeting metabolism with arsenic trioxide and dichloroacetate in breast cancer cells. *Molecular Cancer*, *10*, 142. https://doi.org/10.1186/1476-4598-10-142

Tammi, M. I., Oikari, S., Pasonen-Seppanen, S., Rilla, K., Auvinen, P., & Tammi, R. H. (2018). Activated hyaluronan metabolism in the tumor matrix—Causes and consequences. *Matrix Biology*, *78-79*:147-164.

Tammi, R. H., Passi, A. G., Rilla, K., Karousou, E., Vigetti, D., Makkonen, K., & Tammi, M. I. (2011). Transcriptional and post-translational regulation of hyaluronan synthesis. *The FEBS Journal*, *278*, 1419–1428. https://doi.org/10.1111/j.1742-4658.2011.08070.x

Tiainen, S., Oikari, S., Tammi, M., Rilla, K., Hamalainen, K., Tammi, R., … Auvinen, P. (2016). High extent of O-GlcNAcylation in breast cancer cells correlates with the levels of HAS enzymes, accumulation of hyaluronan, and poor outcome. *Breast Cancer Research and Treatment*, *160*, 237–247. https://doi.org/10.1007/s10549-016-3996-4

Twarock, S., Freudenberger, T., Poscher, E., Dai, G., Jannasch, K., Dullin, C., … Fischer, J. W. (2011). Inhibition of oesophageal squamous cell carcinoma progression by in vivo targeting of hyaluronan synthesis. *Molecular Cancer*, *10*, 30. https://doi.org/10.1186/1476-4598-10-30

Twarock, S., Reichert, C., Peters, U., Gorski, D. J., Rock, K., & Fischer, J. W. (2017). Hyperglycaemia and aberrated insulin signalling stimulate tumour progression via induction of the extracellular matrix component hyaluronan. *International Journal of Cancer Journal International du Cancer*, *141*, 791–804. https://doi.org/10.1002/ijc.30776

Twarock, S., Tammi, M. I., Savani, R. C., & Fischer, J. W. (2010). Hyaluronan stabilizes focal adhesions, filopodia, and the proliferative phenotype in esophageal squamous carcinoma cells. *The Journal of Biological Chemistry*, *285*, 23276–23284. https://doi.org/10.1074/jbc.M109.093146

Vander Heiden, M. G., Cantley, L. C., & Thompson, C. B. (2009). Understanding the Warburg effect: The metabolic requirements of cell

proliferation. *Science*, *324*, 1029–1033. https://doi.org/10.1126/science.1160809

Vernieri, C., Casola, S., Foiani, M., Pietrantonio, F., de Braud, F., & Longo, V. (2016). Targeting cancer metabolism: Dietary and pharmacologic interventions. *Cancer Discovery*, *6*, 1315–1333. https://doi.org/10.1158/2159-8290.CD-16-0615

Vigetti, D., Clerici, M., Deleonibus, S., Karousou, E., Viola, M., Moretto, P., … Passi, A. (2011). Hyaluronan synthesis is inhibited by adenosine monophosphate-activated protein kinase through the regulation of HAS2 activity in human aortic smooth muscle cells. *The Journal of Biological Chemistry*, *286*, 7917–7924. https://doi.org/10.1074/jbc.M110.193656

Vigetti, D., Deleonibus, S., Moretto, P., Karousou, E., Viola, M., Bartolini, B., … Passi, A. (2012). Role of UDP-N-acetylglucosamine (GlcNAc) and O-GlcNAcylation of hyaluronan synthase 2 in the control of chondroitin sulfate and hyaluronan synthesis. *The Journal of Biological Chemistry*, *287*, 35544–35555. https://doi.org/10.1074/jbc.M112.402347

Vigetti, D., Viola, M., Karousou, E., De Luca, G., & Passi, A. (2014). Metabolic control of hyaluronan synthases. *Matrix Biology*, *35*, 8–13. https://doi.org/10.1016/j.matbio.2013.10.002

Warburg, O. (1956). On the origin of cancer cells. *Science*, *123*, 309–314. https://doi.org/10.1126/science.123.3191.309

Yi, W., Clark, P. M., Mason, D. E., Keenan, M. C., Hill, C., Goddard, W. A. 3rd, … Hsieh-Wilson, L. C. (2012). Phosphofructokinase 1 glycosylation regulates cell growth and metabolism. *Science*, *337*, 975–980. https://doi.org/10.1126/science.1222278

Yoshihara, S., Kon, A., Kudo, D., Nakazawa, H., Kakizaki, I., Sasaki, M., … Takagaki, K. (2005). A hyaluronan synthase suppressor, 4-methylumbelliferone, inhibits liver metastasis of melanoma cells. *FEBS Letters*, *579*, 2722–2726. https://doi.org/10.1016/j.febslet.2005.03.079

Zhou, X., Chen, R., Yu, Z., Li, R., Li, J., Zhao, X., … Huang, G. (2015). Dichloroacetate restores drug sensitivity in paclitaxel-resistant cells by inducing citric acid accumulation. *Molecular Cancer*, *14*, 63. https://doi.org/10.1186/s12943-015-0331-3

SUPPORTING INFORMATION

Additional supporting information may be found online in the Supporting Information section at the end of the article.

How to cite this article: Twarock S, Reichert C, Bach K, et al. Inhibition of the hyaluronan matrix enhances metabolic anticancer therapy by dichloroacetate in vitro and in vivo. *Br J Pharmacol*. 2019;176:4474–4490. https://doi.org/10.1111/bph.14808